Renewable Energy 35 (2010) 2468–2475

Contents lists available at ScienceDirect

Renewable Energy

journal homepage: www.elsevier.com/locate/renene

Determination of the optimal tilt angle and orientation for solar photovoltaic arrays

E.D. Mehleri, P.L. Zervas, H. Sarimveis*, J.A. Palyvos, N.C. Markatos

National Technical University of Athens, School of Chemical Engineering, 9 Heroon Polytechniou Str., Zografou University Campus, GR-15780 Athens, Greece

ARTICLE INFO

Article history:
Received 10 November 2009
Accepted 6 March 2010
Available online 1 April 2010

Keywords:
Photovoltaic systems
Global solar irradiance
Optimization
Tilt angle
Orientation
Radial basis function (RBF)

ABSTRACT

This paper deals with the determination of optimum tilt angle and orientation for solar photovoltaic arrays in order to maximize incident solar irradiance exposed on the array, for a specific period of time. The method is extended, by introducing a second objective, i.e. minimization of variance of the produced power, in terms of hourly power generation throughout the given period of time. The proposed method uses both well-established models and data collected from the particular area where the photovoltaic panels will be installed and is built upon four steps. In the first step, the recorded data are used in order to select the most accurate, among several isotropic and anisotropic models that can be found in the literature, for predicting diffuse solar irradiance on inclined surfaces. In the second step, the recorded data and the selected model are used to construct a database that contains the averages and the variances of the hourly global solar irradiance on tilted surfaces over specific periods of time, for various tilt angles and orientations. In the third step, the database of the previous step is utilized to produce metamodels that correlate tilt angle and orientation with mean global irradiance and its variance on tilted surfaces. Finally, an optimization problem is formulated, aiming to determining the optimum values of tilt angle and orientation, taking into account the constraints and limitations of the system.

1. Introduction

The increase of the energy consumption in addition to the need for reducing the emission of pollutants into the atmosphere by using renewable energy sources, has led to a tremendous increase in the use of Photovoltaic (PV) systems [1,2].

A key objective when installing a photovoltaic panel is to achieve the maximum energy output and to avoid shading. To intercept the maximum sunlight, a PV panel must be positioned so that the sun rays arrive at the panel vertically. If not, it does not produce as much power as it could. In order to collect the maximum possible daily energy, one solution is to use tracking systems [3]. A tracker is a mechanical device that follows the direction of the sun on its daily sweep across the sky. However, trackers are expensive and are not always applicable [4]. Thus, in many applications, fixed installations or installations where tilt angle can be adjusted manually are used. It is clear, that in such cases maximum power production can be achieved if the optimal values of tilt and azimuth angles can be determined.

For solar energy applications in the northern hemisphere, optimum orientation is considered to be that of due south. In most cases, PV panels are placed according to this general rule [5,6]. However, there are cases, such as in building-integrated photovoltaic systems (BIPV), where photovoltaic modules are placed in an off-south-facing position, usually according to the façade types and architecture arts [7]. As far as the optimum tilt angle is concerned, this depends on the local latitude. As a rule of thumb, photovoltaics are usually positioned at a tilt angle approximately equal to the latitude of the site and facing south.

Many studies have been performed in order to select the ideal tilt angle of PV panels, based on observation of specific diagrams, empirical relationships and by taking into account detailed characteristics of the site of installation [8–11]. Furthermore, many theoretical models have been suggested by researchers that lead to optimum tilt angles of solar collectors [12–14]. However, the majority of these studies consider the azimuth angle fixed. Obviously, the results can be improved by using two degrees of freedom, i.e. when the design is performed by considering both tilt angle and orientation as free variables.

This paper deals with the determination of both optimum tilt angle and orientation for solar photovoltaic arrays in order to maximize incident solar irradiance exposed on the array, for a specific period of time. The method is extended, by introducing a second

* Corresponding author. Tel.: +30 210 7723237; fax: +30 210 7723138.
E-mail address: hsarimv@chemeng.ntua.gr (H. Sarimveis).

0960-1481/$ – see front matter © 2010 Elsevier Ltd. All rights reserved.
doi:10.1016/j.renene.2010.03.006

objective, i.e. minimization of variance of the produced power, in terms of hourly power generation throughout the given period of time. This objective is important when we are mostly concerned about satisfying power demands with small variations [15]. The proposed method uses both well-established models and data collected from the particular area, where the photovoltaic panels will be installed and was built upon four steps.

As a first step, the model for predicting global solar irradiance on inclined surfaces was selected. Standard formulas were used for simulating the beam and the reflective components. As far as the diffuse component is concerned, several isotropic and anisotropic models were tested using data that have been collected at the National Technical University of Athens (NTUA) station (37°58′26″B, 23°47′16″A, 219 m above mean sea level). The most accurate model was selected for further study. The result of the first step is a model that can predict hourly global solar irradiance on tilted surface at the specific location where data have been collected, given the tilt angle, the orientation, and the time.

In the second step, the selected model was used to calculate the mean value and the variance of the hourly global solar irradiance on tilted surfaces over a year for a wide range of tilt (0°–90°) and azimuth angles (0° to ±60°). The possibility to change the tilt angle twice a year (summer: April–September and winter: October–March), led to the separate investigation of the hot period and the cold period. A database was thus generated that contains mean values and variances of the hourly global solar irradiance on tilted surfaces for several pairs of tilt angles and azimuth angles.

In the third step mathematical relationships were developed between the design variables (tilt angle and azimuth angle) and output variables (mean value and variance of global irradiance on tilted surfaces), using the database that was generated in the previous step. In particular, the linear regression methodology and the radial basis-function (RBF) neural network architecture were utilized for producing the input–output "meta-models". Several statistical tests were used to validate the produced models, illustrating that the nonlinear approach is the most accurate.

Finally, in order to obtain optimal values for tilt and azimuth angles, a Nonlinear programming (NLP) problem was formulated that takes into account the constraints and limitations of the system.

The methodology offers a new tool to PV system designers, since it incorporates two objectives (maximization of the produced power and minimization of variation in power production), optimizes the design with respect to two parameter, and takes into account the particularities of the system and the climatological and geographical characteristics of the particular location.

2. Recorded data

The data used in this study were recorded at the weather station of the National Technical University of Athens (37°58′26″B, 23°47′16″A, 219 m above mean sea level). These data are values over ten-minute intervals of global, beam, and diffuse irradiance on a horizontal surface, as well as global irradiance on a tilted surface (32°), throughout an one-year period (January 2004 to December 2004) which were then transformed into hourly values, Finally, the available data set contained 8760×4 values and covered a full calendar year. The experimental values for global, diffuse, and beam irradiance on a horizontal surface and the global irradiance on a tilted surface are denoted by I_i, $I_{b,i}$, $I_{d,i}$, $I_{t,i}$ respectively for $i = 1,2,\ldots,8760$.

3. Selection of the model for predicting global solar irradiance on tilted surface(s)

The hourly global solar irradiance incident on inclined surfaces I_t is composed of the beam (I_{tb}), diffuse (I_{td}), and ground-reflected (I_{tr}) components. The beam and ground-reflected components were calculated by using simple models found in the literature [16,17]. The nature of the diffuse component is more complicated and needs more attention.

In particular, the equations for simulating the *beam component* are presented below:

$$I_{tb} = I_b \cdot R_b \tag{1}$$

$$R_b = \cos t_h / \cos t_{hz} \tag{2}$$

$$\cos t_{hz} = \sin\varphi \cdot \sin\delta \cdot \cos\varphi \cdot \cos\delta \cdot \cos\omega \tag{3}$$

$$\begin{aligned} \cos t_h = {} & \sin\delta \cdot \sin\varphi \cdot \cos b - \sin\delta \cdot \cos\varphi \cdot \sin b \cdot \cos g \\ & + \cos\delta \cdot \cos\varphi \cdot \cos b \cdot \cos\omega \\ & + \cos\delta \cdot \sin\varphi \cdot \sin b \cdot \cos g \cdot \cos\omega \\ & + \cos\delta \cdot \sin b \cdot \sin g \cdot \sin\omega \end{aligned} \tag{4}$$

$$\delta = 23.45 \cdot \sin[2\pi \cdot (284 + n)/365] \tag{5}$$

where I_{tb} is the hourly beam irradiance on inclined surfaces, t_{hz} is the solar zenith angle, t_h is the solar incidence angle on a tilted plane, φ is the latitude of the location, δ is the solar declination, b is the tilt angle, ω is the solar hour angle, g is the azimuthal angle and n is the day of the year starting from the 1st of January.

The solar hour angle ω is defined as the angular displacement of the sun on the apparent orbit (ecliptic) east or west of the local meridian (it is zero at solar noon and varies by 15° per hour from solar noon, it is negative in the morning and positive in the afternoon). The azimuth angles for the northern hemisphere, range between −90° and 90° (i.e. $g = 0°$ for south-facing, $g = -90°$ for east-facing, $g = 90°$ for west-facing surfaces).

The *ground-reflected* component was computed by the following formula

$$I_{tr} = 1/2 \cdot r_g \cdot I \cdot (1 - \cos b) \tag{6}$$

where r_g is the ground reflectivity and I is the global solar irradiance on horizontal surfaces.

It must be noted that the aforementioned method presumes that the components of global solar irradiance on the horizontal surface are known. If not, the appropriate decomposition model should be selected for their calculation [18]. Furthermore, in remote areas where data of global solar irradiance is sparse or unavailable, many studies found in the literature can provide accurate predictions [19,20].

As far as the diffuse component is concerned, several empirical methods can be found in the literature, which can be classified as isotropic and anisotropic. The isotropic models assume the uniformity of diffuse sky irradiance over the sky dome. The anisotropic models assume the anisotropy of the diffuse sky irradiance in the circumsolar region (sky near the solar disk) and an isotropically diffuse component for the rest of the sky dome. The diffuse models that appear in Table 1 were tested on the collected data (see Section 2) as follows: For each one of the 8760 recorded values an estimate of the hourly global irradiance on a tilted surface of 32° was produced using the following equation:

$$\widehat{I}_{t,i} = I_{tb,i} + I_{tr,i} + \widehat{I}_{td,i} \tag{7}$$

where $I_{tb,i}$, $I_{tr,i}$ were calculated by Eqs. (1)–(5) and (6) respectively for $i = 1,2,\ldots,8760$, while $\widehat{I}_{td,i}$ is the prediction of the diffuse model that was tested. The predictions obtained by Eq. (7) were tested against the experimental $I_{t,i}$ values for each possible choice for

Table 1
Statistical comparison of various hourly slope irradiation models.

1. Isotropic – Liu and Jordan, 1962	$R^2 = 0.938$, $RMSE = 0.085$, $MBE\% = 6.995$, $MBE = 0.032$, $MPE = 7$, $t\text{-}stat = 25.9$
2. Isotropic – Koronakis, 1986	$R^2 = 0.938$, $RMSE = 0.087$, $MBE\% = 8.829$, $MBE = 0.036$, $MPE = 7.8$, $t\text{-}stat = 28.9$
3. Isotropic – Badescu, 2002	$R^2 = 0.935$, $RMSE = 0.082$, $MBE\% = 5.738$, $MBE = 0.023$, $MPE = 4.934$, $t\text{-}stat = 18.238$
4. Isotropic – Tian, 2001	$R^2 = 0.934$, $RMSE = 0.081$, $MBE\% = 4.388$, $MBE = 0.017$, $MPE = 3.739$, $t\text{-}stat = 13.721$
5. Anisotropic – Bugler, 1977	$R^2 = 0.937$, $RMSE = 0.089$, $MBE\% = 9$, $MBE = 0.037$, $MPE = 8.18$, $t\text{-}stat = 29.3$
6. Anisotropic – Reindl, 1990	$R^2 = 0.934$, $RMSE = 0.097$, $MBE\% = 10.719$, $MBE = 0.044$, $MPE = 10.307$, $t\text{-}stat = 33.165$
7. Anisotropic – Temps and Coulson, 1977	$R^2 = 0.938$, $RMSE = 0.098$, $MBE\% = 12.443$, $MBE = 0.053$, $MPE = 11.43$, $t\text{-}stat = 40.917$
8. Anisotropic – Klucher, 1979	$R^2 = 0.939$, $RMSE = 0.099$, $MBE\% = 12.719$, $MBE = 0.054$, $MPE = 12.13$, $t\text{-}stat = 41.265$
9. Anisotropic – Ma and Iqbal	$R^2 = 0.926$, $RMSE = 0.108$, $MBE\% = 13.537$, $MBE = 0.058$, $MPE = 12.637$, $t\text{-}stat = 40.606$
10. Anisotropic – Jimenez and Castro, 1986	$R^2 = 0.869$, $RMSE = 0.123$, $MBE\% = -10{,}789$, $MBE = -0.036$, $MPE = -4.569$, $t\text{-}stat = 19.645$
11. Anisotropic – Iqbal, 1983	$R^2 = 0.8$, $RMSE = 0.243$, $MBE\% = 31.3$, $MBE = 0.17$, $MPE = 31.4$, $t\text{-}stat = 62.5$

modeling the diffuse component. The results are summarized in Table 1, where the following statistical indices are shown: the coefficient of multiple determination R^2, the root mean square error (RMSE), the mean bias error (MBE), the mean percentage error (MPE) and the statistical index (t-stat) [21]. The most accurate results were produced, when the isotropic model of "Liu and Jordan" [22] was used for predicting the diffuse component. Therefore, this model was utilized for simulating the diffuse component for the rest of this study.

4. Construction of the database

The model described in the previous section was used to construct a database that contains means and variances of hourly global solar irradiance estimates on inclined surfaces for various tilt angles and orientations. Different databases were generated for the full calendar year, the hot season and the cold season, using the full set or subsets of the 8760 time periods that describe a calendar year. The values of the tilt angles ranged between 0° and 90°, using a step of 5°, while the angles of orientation were varied in the range 0° to ±60° with a step of 5°. Standard formulas for calculating the sample means and variances were used. For example, the sample means and variances for the full calendar year were calculated as follows:

Table 2
The database containing average values and variances of global solar irradiance on inclined surfaces over a full calendar year.

No. of data	b	g	$\bar{I}_t$	Var
1	0	−60	0.40092	0.019737
…	…	…	…	…
35	5	−15	0.41179	0.018217
36	5	−10	0.4124	0.018183
37	5	−5	0.41293	0.018161
…	…	…	…	…
475	90	60	0.28382	0.001443

$$\bar{I}_t = \left(\frac{1}{8760}\cdot\sum_{i=1}^{8760}\hat{I}_{t,i}\right) \tag{8}$$

$$Var = \left(\frac{1}{(8760-1)}\cdot\sum_{i=1}^{8760}\left(\hat{I}_{t,i}-\bar{I}_t\right)^2\right) \tag{9}$$

and the results are tabulated in matrix form as shown in Table 2. Similar tables were produced for the hot and the cold period, considering only the data corresponding to the months April–September for the hot period and October–March for the cold period.

5. Development of the meta-models

This section describes the procedure that was followed in order to construct correlation equations, based on the databases developed in the previous section: In particular, correlation equations were developed among the design variables, b, g (input variables) and the mean value $\bar{I}_t$ and variance Var of the hourly global solar irradiance on inclined surfaces, which were considered as output variables. The three different periods (entire year, hot period, and cold period) were studied separately and different models were developed for each period. Two modeling methodologies were used, namely standard multiple linear regression (MLR) and the radial basis-function neural network architecture.

5.1. Linear regression

For each period (full year, hot period, cold period) a trial and error procedure was used to derive the best possible linear models. The linear (in terms of coefficients) equations, along with the respective statistical indices are shown in Table 3.

Table 3
Linear equations correlating the design parameters b, g with $\bar{I}_t$ and Var for the three periods under study.

First period: the entire year	$\hat{\bar{I}}_t = -8.51824\times10^{-6}\cdot g^2 - 3.71813\times10^{-5}\cdot b^2 + 3.62263\times10^{-4}\cdot g + 1.86553\times10^{-3}\cdot b + 0.41462$	$R^2 = 0.9785$ $RSS = 2.6382\times10^{-2}$ $S = 7.4921\times10^{-3}$
	$\widehat{Var} = 6.5529\times10^{-7}\cdot g^2 + 2.17097\times10^{-6}\cdot b^2 - 5.20045\times10^{-6}\cdot g - 4.13949\times10^{-4}\cdot b + 0.01976$	$R^2 = 0.99$ $RSS = 1.77965\times10^{-4}$ $S = 6.1535\times10^{-4}$
Second period: hot season	$\hat{\bar{I}}_t = -8.62797\times10^{-6}\cdot g^2 - 3.86732\times10^{-5}\cdot b^2 + 3.05632\times10^{-4}\cdot g + 6.00177\times10^{-4}\cdot b + 0.52590$	$R^2 = 0.9912$ $RSS = 2.9386\times10^{-2}$ $S = 7.9072\times10^{-3}$
	$\widehat{Var} = 8.77731\times10^{-7}\cdot b^2 - 2.06613\times10^{-6}\cdot g - 1.38212\times10^{-4}\cdot b + 5.95969\times10^{-3}$	$R^2 = 0.9779$ $RSS = 3.2011\times10^{-5}$ $S = 2.607\times10^{-4}$
Third period: cold season	$\hat{\bar{I}}_t = -1.61733\times10^{-5}\cdot g^2 - 3.56904\times10^{-5}\cdot b^2 + 4.18891\times10^{-4}\cdot g + 3.13102\times10^{-3}\cdot b + 0.30332$	$R^2 = 0.894$ $RSS = 6.503\times10^{-2}$ $S = 1.1763\times10^{-2}$
	$\widehat{Var} = -2.05642\times10^{-8}\cdot g^2 - 1.51857\times10^{-7}\cdot b^2 + 1.49806\times10^{-6}\cdot g - 2.00623\times10^{-5}\cdot b + 4.27873\times10^{-3}$	$R^2 = 0.9792$ $RSS = 8.7433\times10^{-6}$ $S = 1.3639\times10^{-4}$

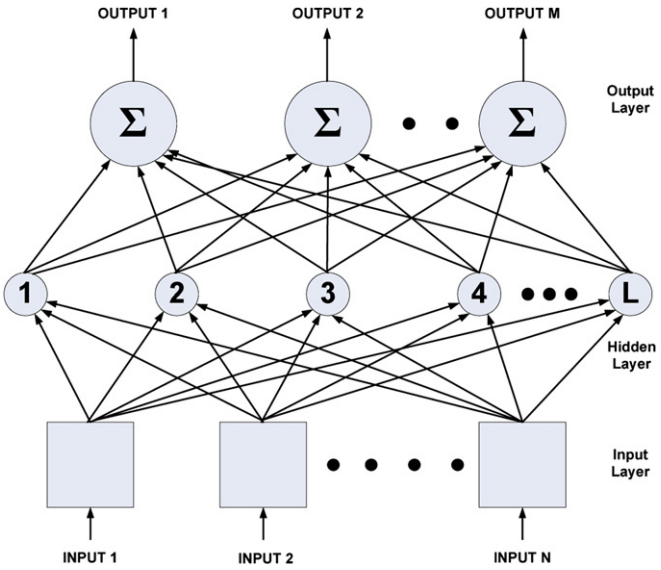

Fig. 1. Standard topology of an RBF neural network.

In the above equations, R^2 is the coefficient of multiple determination, *RSS* is the residual sum of squares and *S* the standard deviation.

5.2. Neural network model (NNM)

In order to further increase the accuracy of the produced models, a nonlinear statistical modeling approach, namely the RBF neural network architecture was utilized for deriving regression equations. This specific architecture was chosen because of its simple topology and the fast and robust algorithms available in the literature for training such networks. The radial basis-function network consists of an input layer, an output layer and one hidden layer in which the activation function is typically Gaussian function [23], as presented in Fig. 1.

In the present work, the RBF neural network is structured so that it can predict the mean global solar irradiance on inclined surfaces, $\bar{I}_t$, or the variance *Var* as output variables, using two independent input parameters: the tilt angle, *b*, and the orientation, *g*. Thus the input vector *x* is defined as $x = [b, g]^T$.

The neural network output provides a prediction of the output and is calculated as the weighted summation of the responses of the hidden layers. For, example the prediction for the mean value $\widehat{\bar{I}}_t$

$$\widehat{\bar{I}}_t = \sum_{j=1}^{L} w_j z_j(x) \tag{10}$$

where $z_j(x) = f(\|x - x_j\|_2^2)$

In the above equations z_j is the response of the *j*th node, *f* is the radial basis function, x_j is the centre of the *j*th node, *L* is the total number of hidden nodes and w_j is the weight corresponding to the response of the *j*th node.

An RBF training procedure, aims at the determination of the number of nodes in the hidden layer, the hidden node centres and the output weights, in order to minimize the deviation between the measured and predicted values of the output variables over the set of the available database. The training method used in this work is the fuzzy-means algorithm, which is presented in details in [24]. The training procedure was used several times by altering at each run the fuzzy partition of the input space (number of fuzzy sets defined in each input dimension), which is in fact the only design parameter that must be defined by the user when utilizing the fuzzy-means algorithm. Due to space limitations the produced RBF models are not shown in the paper, but they can be available to the interested readers. For the same reason, only the results corresponding to the full time period are presented in details.

Both modeling methodologies were validated by randomly partitioning the data into training and validation sets (75% and 25% of the data, respectively). The modeling methodologies were applied on the training data and the produced models were tested on the validation data set. As far as the RBF modeling methodology is concerned, different neural network models were developed by altering the fuzzy partition of the input space. The results for the full calendar year are summarized in Tables 4 and 5 along with the statistical indices: residual sum of squares (*RSS*), the coefficient of multiple determination R^2 and standard deviation *S*.

The higher R^2 values and the lower *RSS* and *S* values in Tables 4 and 5, make it clear that the prediction accuracy of the RBF models is superior to the model produced using the MLR methodology. Among the RBF models, the prediction results (predictions over the validation set) were gradually improved up to the point where ten fuzzy sets were used to partition the domain of each input variable for full year. A further increase results to the overtraining phenomenon, where the performance of the produced model is not improved, although the model increases in size.

The above discussion can be supported by a visual representation of the prediction results. Figs. 2 and 3 plot the predictions of the MLR models and the best RBF models for mean value and average against the respective database values. It is clear that the predicted vs. actual points in the RBF plots are closer to the main diagonal, thus illustrating the higher accuracy of the RBF models. Therefore, the RBF models generated using a fuzzy partition of each input variable into 10 fuzzy sets were used in the formulation of the optimization problems that will be presented in the next section of this work.

As mentioned above, due to space limitations the results corresponding to the hot or cold periods are not presented in details. The same approach was followed, with very similar results, i.e. neural network models generated by considering the partition of each input dimension into 10 fuzzy sets were finally selected for predicting the mean value and the average of global solar irradiance on tilted surfaces for the hot and the cold period.

6. Formulation of the optimization problems

This section presents the procedure that was followed to determine the optimum pair of tilt angle and orientation of the photovoltaic array. The definition of the objective function is crucial in the formulation of the optimization problem. The key term that

Table 4
Performance of full period MLR and RBF models predicting I_t on the validation data set.

	Linear model	RBF (7 fuzzy sets)	RBF (8 fuzzy sets)	RBF (9 fuzzy sets)	RBF (10 fuzzy sets)
R^2	0.9785	0.9949	0.9998	0.9995	0.9999
RSS	2.6382×10^{-2}	3.4679×10^{-3}	1.4668×10^{-4}	3.3101×10^{-5}	2.8519×10^{-5}
S	7.4921×10^{-3}	3.5972×10^{-3}	7.3981×10^{-4}	1.1113×10^{-3}	3.2627×10^{-4}

Table 5
Performance of full period MLR and RBF models predicting variance on the validation data set.

	Linear model	RBF (7 fuzzy sets)	RBF (8 fuzzy sets)	RBF (9 fuzzy sets)	RBF (10 fuzzy sets)
R^2	0.9900	0.9986	0.9995	0.9997	0.9999
RSS	1.7796×10^{-4}	5.4231×10^{-6}	5.2393×10^{-6}	2.9192×10^{-6}	1.1196×10^{-6}
S	6.1535×10^{-4}	2.3045×10^{-4}	1.3984×10^{-4}	1.0440×10^{-4}	6.4623×10^{-5}

should be maximized is global irradiance on the tilted surface, which is proportional to the output power of the photovoltaic power generation (*ppv*) [19]. However, in particular applications, the variance in the power production should be kept at low levels. This objective is taken into account by introducing the variance as a second term in the objective function with a negative sign. The second objective is weighted with respect to the first objective.

For a through presentation of the optimization problems that will be formulated next, we summarize at this point the models that have been developed for predicting the mean value and the variance of the global solar irradiance on tilted surfaces for the full period, the hot period and the cold period.

$$\hat{\bar{I}}_{t,f} = RBF_{f,1}(b,g) \tag{11}$$

$$\widehat{Var}_f = RBF_{f,2}(b,g) \tag{12}$$

$$\hat{\bar{I}}_{t,h} = RBF_{h,1}(b,g) \tag{13}$$

$$\widehat{Var}_h = RBF_{h,2}(b,g) \tag{14}$$

$$\hat{\bar{I}}_{t,c} = RBF_{c,1}(b,g) \tag{15}$$

$$\widehat{Var}_c = RBF_{c,2}(b,g) \tag{16}$$

In the above models the subscript f refers to the full period, the subscript h to the hot period and the subscript c to the cold period.

The first optimization problem assumes a fixed tilt angle and orientation throughout the calendar year: The problem is described by the following maximization model

$$\max_{b,g}\left(\hat{\bar{I}}_{t,f} - \varepsilon\cdot\widehat{Var}_f\right) \tag{17}$$

subject to the constraints posed by the RBF models that predict $\hat{\bar{I}}_{t,f}$, $\widehat{Var}_f$ as functions of b and g. The following upper and lower limits were additionally posed on the tilt angle and the orientation:

$$0^\circ \le b \le 90^\circ \tag{18}$$

$$-60^\circ \le g \le 60^\circ \tag{19}$$

The next formulation of the optimization problem considers the possibility of changing the tilts angle twice per year (i.e. different tilt angles for the hot and the cold periods), keeping the orientation fixed. The full description of the optimization problem follows next:

$$\max_{b_c,b_h,g}\frac{1}{2}\left(\hat{\bar{I}}_{t,c} + \hat{\bar{I}}_{t,h} - \varepsilon\cdot\widehat{Var}_c - \varepsilon\cdot\widehat{Var}_h\right) \tag{20}$$

$$\hat{\bar{I}}_{t,h} = RBF_{h,1}(b_c,g) \tag{21}$$

$$\widehat{Var}_h = RBF_{h,2}(b_c,g) \tag{22}$$

$$\hat{\bar{I}}_{t,c} = RBF_{c,1}(b_h,g) \tag{23}$$

$$\widehat{Var}_c = RBF_{c,2}(b_h,g) \tag{24}$$

$$0^\circ \le b_c \le 90^\circ \tag{25}$$

$$0^\circ \le b_h \le 90^\circ \tag{26}$$

$$-60^\circ \le g \le 60^\circ \tag{27}$$

In the above formulation the objective function contains the predictions of mean values and variances of global irradiance on tilted surfaces for both the hot and the cold periods. It should be noted that there are three design parameters in this formulation, namely the tilt angles in the hot and cold periods b_h, b_c and the fixed azimuth angle g.

Another alternative formulations concerns photovoltaic applications in buildings, where the orientation is predetermined, i.e. g is no longer a design parameter. Both formulations can be adjusted

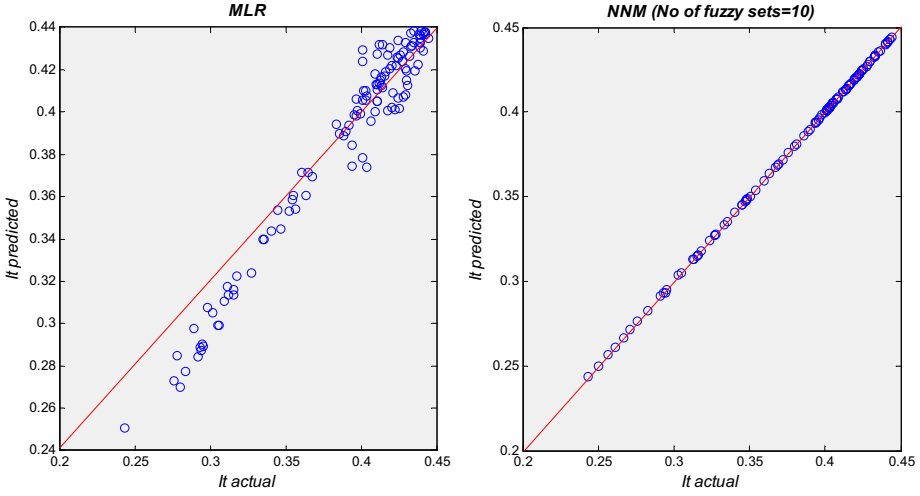

Fig. 2. Actual I_t values vs predicted values for the validation data set/full period.

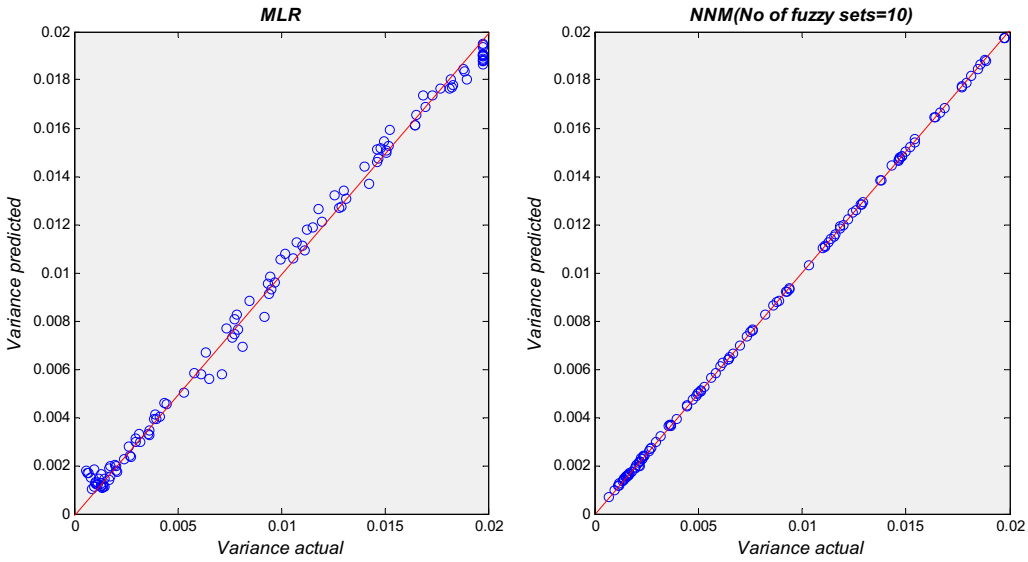

Fig. 3. Actual values of variance vs predicted values for the validation data set/full period.

Table 6
Optimization results for fixed tilt angle.

Objective function	Value of objective function	b	g	ppv (kW/m^2)	Loss of ppv (%)
$\bar{I}_{t,f} - 0\cdot\widehat{Var}_f$	0.4446	30	15	0.0528	0
$\bar{I}_{t,f} - 10\cdot\widehat{Var}_f$	0.3553	51	−16	0.0477	−9.7
$\bar{I}_{t,f} - 20\cdot\widehat{Var}_f$	0.3182	60	−25	0.0437	−17.23
$\bar{I}_{t,f} - 30\cdot\widehat{Var}_f$	0.2945	64	−29	0.0416	−21.21
$\bar{I}_{t,f} - 40\cdot\widehat{Var}_f$	0.2758	68	−28	0.0401	−24.00
$\bar{I}_{t,f} - 50\cdot\widehat{Var}_f$	0.2597	72	−25	0.0386	−26.90
$\bar{I}_{t,f} - 60\cdot\widehat{Var}_f$	0.2456	75	−23	0.0376	−28.79
$\bar{I}_{t,f} - 70\cdot\widehat{Var}_f$	0.2330	78	−21	0.0364	−31.06

to this particular case by removing g from the design parameter set and using the predetermined value of g in Eq. (17) or (20).

The nonlinear neural programming problems that are formulated are solved using GAMS [25].

7. Results and discussion

This section presents the results obtained from the solutions of the aforementioned optimization frameworks. The optimization procedure was performed for different weights on the variance term that range between 0 and 70. For each weight value, the optimum tilt angle(s) and orientation were obtained. The results are summarized in Table 6 for the case where a fixed tilt angle is used throughout the year (case 1) and in Table 7 for the case where different tilt angles are used in the hot and the cold period (case 2). The photovoltaic power generation (ppv) was calculated with an empirical model which expresses ppv as a function of I_t and the ambient temperature (T_{amb}) [19].

Table 7
Optimization results for different tilt angles in hot and cold season.

Objective function	Value of objective function	b_h	b_c	g	ppv (kW/m^2)	Loss of ppv (%)
$1/2(\bar{I}_{t,c} + \bar{I}_{t,h} - 0\cdot\widehat{Var}_c - 0\cdot\widehat{Var}_h)$	0.4587	15	50	15	0.0546	
$1/2(\bar{I}_{t,c} + \bar{I}_{t,h} - 10\cdot\widehat{Var}_c - 10\cdot\widehat{Var}_h)$	0.4253	20	52	14	0.0544	−0.37
$1/2(\bar{I}_{t,c} + \bar{I}_{t,h} - 20\cdot\widehat{Var}_c - 20\cdot\widehat{Var}_h)$	0.3960	25	53	10	0.0534	−2.19
$1/2(\bar{I}_{t,c} + \bar{I}_{t,h} - 30\cdot\widehat{Var}_c - 30\cdot\widehat{Var}_h)$	0.3725	32	60	−10	0.0520	−4.76
$1/2(\bar{I}_{t,c} + \bar{I}_{t,h} - 40\cdot\widehat{Var}_c - 40\cdot\widehat{Var}_h)$	0.3532	40	70	−15	0.0502	−8.06
$1/2(\bar{I}_{t,c} + \bar{I}_{t,h} - 50\cdot\widehat{Var}_c - 50\cdot\widehat{Var}_h)$	0.3366	40	72	−20	0.0488	−10.62
$1/2(\bar{I}_{t,c} + \bar{I}_{t,h} - 60\cdot\widehat{Var}_c - 60\cdot\widehat{Var}_h)$	0.3246	42	77	−30	0.0476	−12.82
$1/2(\bar{I}_{t,c} + \bar{I}_{t,h} - 70\cdot\widehat{Var}_c - 70\cdot\widehat{Var}_h)$	0.3108	45	80	−32	0.0459	−15.94

The last columns of Tables 6 and 7, compare the results obtained by considering only the average global solar irradiance on the tilted surface ($\varepsilon = 0$) to the results corresponding to different levels of the weight factor. It is clear that when variance is included in the objective function, the produced power is reduced. However this power loss is much lower when different tilt angles are used in the hot and the cold period (case 2). One additional observation is the considerable change on optimal values of both tilt angles and orientation as the weight of variance increases. The range of optimal tilt angle values is wider in case 1 (the optimal b values range between 30° and and 78°) compared to case 2 (the optimal b_h values range between 15° and and 45°, while the range for the optimal b_c is [50°, 80°]). The opposite happens for the optimal g values (the ranges are [15°, −21°] for case 1 and [15°, −32°] for case 2). It is also important to note that in case 2 the optimal tilt angle for the cold period is always larger to the optimal value in the hot period, regardless of the weight that penalizes variance in the objective function.

As far as the comparison of the two cases is concerned, the change of the tilt angles twice a year, increases the power output of the photovoltaic array by 3.5% when lack of uniformity is not penalized ($\varepsilon = 0$), to 26% when variance is penalized with the highest weight ($\varepsilon = 70$). It should be noted that when the tilt angle is fixed throughout the year (case 1), the produced ppv for $\varepsilon = 0$ is lower compared to the case where different angles of the PV panels are used in the hot and the cold period (case 2), even when variance is penalized by a weight factor up to 20 in the objective function.

Summarizing, the results show that the possibility of changing the tilt angle of the photovoltaic array in the cold and hot season clearly improves considerably the performance and uniformity of the power output of the photovoltaic array.

8. Conclusions

In this work a new methodology was presented for the computation of the optimal tilt angle and orientation of a photovoltaic array at a specific location.

In the first part of the paper, several models that have been proposed in the literature for predicting the diffuse component of the global solar irradiance on a tilted surface were tested based on experimental data. The most accurate model of "Liu and Jordan" was selected and by combining it with standard formulas for the two remaining components (beam and ground-reflected), a complete model for predicting global solar irradiance on tilted surfaces was derived.

In the second part, the mean values and the averages of global solar irradiance on tilted surfaces were calculated using the aforementioned model. Calculations were performed for the full calendar year, but also considering only the hot or cold periods.

Then, the linear regression methodology and the RBF neural network architecture were used to develop meta-models that correlate the design parameters (i.e. tilt angle and orientation) with the mean value and the variance of global irradiance on tilted surfaces. The nonlinear approach proved superior compared to the linear method.

In the last part of the study, two optimization problems were formulated in order to maximize the produced power of the photovoltaic array, taking into account the uniformity of the produced power. The results show that the possibility of changing the tilt angle and of the photovoltaic array in the cold and hot seasons would improve the quantity and uniformity of the produced power.

In conclusion, the proposed methodology may be a useful tool for researchers and designers interested in installing photovoltaic arrays, since it can yield the optimal tilt angle and orientation, taking into account the design specifications.

Appendix. Nomenclature

b	Tilt angle (°)
b_c	Tilt angle for the cold season (°)
b_h	Tilt angle for the hot season (°)
f	Radial basis function
g	Orientation (azimuthal angle) (°)
I	Global solar irradiance on a horizontal surface (kW/m^2)
I_i	Global solar irradiance on a horizontal surface for the ith observation (kW/m^2)
I_b	Beam irradiance on a horizontal surface (kW/m^2)
$I_{b,i}$	Beam irradiance on a horizontal surface for the ith observation (kW/m^2)
I_d	Diffuse irradiance on a horizontal surface (kW/m^2)
$I_{d,i}$	Diffuse irradiance on a horizontal surface for the ith observation (kW/m^2)
I_t	Global solar irradiance on inclined surfaces (kW/m^2)
$I_{t,i}$	Global solar irradiance on inclined surfaces for the ith observation (kW/m^2)
$\widehat{I}_{t,i}$	Predicted value of global solar irradiance on inclined surfaces for the ith observation (kW/m^2)
$\overline{I_t}$	Mean global solar irradiance on inclined surfaces (kW/m^2)
$\widehat{\overline{I}}_t$	Model prediction of mean global solar irradiance on inclined surfaces (kW/m^2)
$\widehat{\overline{I}}_{t,c}$	Model prediction of mean solar irradiance on inclined surfaces for the cold season (kW/m^2)
$\widehat{\overline{I}}_{t,f}$	Model prediction of mean solar irradiance on inclined surfaces for the full season (kW/m^2)
$\widehat{\overline{I}}_{t,h}$	Model prediction of mean solar irradiance on inclined surfaces for the cold season (kW/m^2)
I_{tb}	Beam irradiance on an inclined surface for the ith observation (kW/m^2)
$I_{tb,i}$	Beam irradiance on an inclined surface for the ith observation (kW/m^2)
I_{td}	Diffuse irradiance on an inclined surface for the ith observation (kW/m^2)
$\widehat{I}_{td,i}$	Predicted value of diffuse irradiance on inclined surfaces for the ith observation (kW/m^2)
I_{tr}	Ground-reflected irradiance on inclined surfaces for the ith observation (kW/m^2)
$I_{tr,i}$	Ground-reflected irradiance on inclined surfaces for the ith observation (kW/m^2)
L	The number of the hidden nodes
ppv	Photovoltaic power generation (kW/m^2)
R^2	Coefficient of multiple determination
r_g	Ground reflectivity
S	Standard deviation
T_{amb}	Mean ambient temperature (°C)
t_h	Solar incidence angle on a tilted plane (°)
t_{hz}	Solar zenith angle (°)
t-$stat$	Statistical index
Var	Variance of solar irradiance on inclined surfaces (kW/m^2)^2
$\widehat{Var}$	Model prediction of variance of solar irradiance on inclined surfaces (kW/m^2)^2
$\widehat{Var}_c$	Model prediction of variance of solar irradiance on inclined surfaces for the cold period (kW/m^2)^2
$\widehat{Var}_f$	Model prediction of variance of solar irradiance on inclined surfaces for the full period (kW/m^2)^2
$\widehat{Var}_h$	Model prediction of variance of solar irradiance on inclined surfaces for the hot period (kW/m^2)^2
w_j	Weight corresponding to the response of the jth node
x_j	The centre of the jth node
z_j	The response of the jth node
δ	Solar declination (°)
φ	Latitude of the location (°)
ω	Solar hour angle (°)

Abbreviations

MBE	Mean bias error
MPE	Mean percentage error
NLP	Nonlinear programming
NNM	Neural network model
PV	Photovoltaic
RBF	Radial basis function
RMSE	Root mean square error
RSS	The residual sum of squares

References

[1] Jager-Waldau Arnulf. Photovoltaics and renewable energies in Europe. Renewable and Sustainable Energy Reviews 2007;11:1414–37.
[2] Badescu V. Simulation of solar cells utilization on the surface of Mars. Acta Astronautica 1998;43(9–10):443–53.
[3] Sungur Cemil. Multi-axes sun-tracking system with PLC control for photovoltaic panels in Turkey. Renewable Energy 2009;34(4):1119–25.
[4] Nann Stefan. Potentials for tracking photovoltaic systems and V-throughs in moderate climates. Solar Energy 1990;45(6):385–93.
[5] Duffie JA, Beckman WA. Solar engineering of thermal processes. 2nd ed. New York: John Wiley and Sons; 1991.
[6] Lunde PJ. Solar thermal engineering. New York: Wiley; 1980.
[7] Yang H, Lu L. The optimum tilt angles and orientations of PV claddings for building-integrated photovoltaic (BIPV) applications. Journal of Solar Energy Engineering, Transactions of the ASME 2007;129(2):253–5.
[8] Kacira Murat, Simsek Mehmet, Babur Yunus, Demirkol Sedat. Determining optimum tilt angles and orientations of photovoltaic panels in Sanliurfa, Turkey. Renewable Energy 2004;29:1265–75.
[9] Calabro Emanuelle. Determining optimum tilt angles of photovoltaic panels at typical north-tropical latitudes. Journal of Renewable and Sustainable Energy 2009;1:033104.
[10] Shu Naihong, Kameda Nobuhiro, Kishida Yasumitsu, Sonoda Hirotora. Experimental and theoretical study on the optimal tilt angle of photovoltaic panels. Journal of Asian Architecture and Building Engineering 2006;5(2):399–405.

[11] Badescu Viorel. Simple optimization procedure for silicon-based solar cell interconnection in a series-parallel PV module. Energy Conversion and Management 2006;47(9–10):1146–58.
[12] Chang YP. Optimal design of discrete-value tilt angle of PV using sequential neural-network approximation and orthogonal array. Expert Systems with Applications: An International Journal 2009;36(3): 6010–8.
[13] Lewis G. Optimum tilt of solar collector. Solar and Wind Technology 1987;4 (3):407–10.
[14] Balouktsis A, Tsanakas D, Vachtsevanos G. On the optimum tilt angle of a photovoltaic array. International Journal of Sustainable Energy June 1987;5 (3):153–69.
[15] Tsalides Ph, Thanailakis A. Direct computation of the array optimum tilt angle in constant-tilt photovoltaic systems. Solar Cells 1985;14: 83–94.
[16] Noorian Ali Mohammad, Moradi Isaac, Kamali Gholam Ali. Evaluation of 12 models to estimate hourly diffuse irradiation on inclined surfaces. Renewable Energy 2008;33(6):1406–12.
[17] EfimEvseev G, AvrahamKudish I. The assessment of different models to predict the global solar radiation on a surface tilted to the south. Solar Energy 2009;83 (3):377–88.
[18] Mehleri ED, Zervas PL, Sarimveis H, Palyvos JA, Markatos NC. Classification of global solar irradiance decomposition models and development of a new empirical model: implementation for the region of Athens, Greece. In: Proceedings of 10th world renewable energy congress – WREC X, Scotland. 19–25th July 2008.
[19] Zervas PL, Sarimveis H, Palyvos JA, Markatos NC. Model-based optimal control of a hybrid power generation system consisting of photovoltaic arrays and fuel cells. Journal of Power Sources 2008;181:327–38.
[20] Zervas PL, Sarimveis H, Palyvos JA, Markatos NCG. Prediction of daily global solar irradiance surfaces based on neural-network techniques. Renewable Energy 2008;33(8):1796–803.
[21] Stone RJ. Improved statistical procedure for the evaluation of solar radiation estimation models. Solar Energy 1993;51(4):289–91.
[22] Liu BYH, Jordan RC. Daily insolation on surfaces tilted towards the equator. ASHRAE Transactions; 1962:526–41.
[23] Klerfors D. Artificial neural networks. Project MISB-420-0. Saint Louis University; 1998.
[24] Sarimveis H, Alexandridis A, Tsekouras G, Bafas G. Industrial & Engineering Chemistry Research 2002;41:751–9.
[25] Brooke A, Kendrick D, Meeraus A, Raman R. GAMS, user guide. Available with the GAMS system or from, http://www.gams.com; 1998.